Letter

Robust external spin-hyperpolarization of quadrupolar nuclei enabled by strain

Lu Chen,[1,*] Jiawen Jiang,[1,*] Martin B. Plenio,[2] and Qiong Chen[1,†]

[1]*Key Laboratory of Low-Dimension Quantum Structures and Quantum Control of Ministry of Education, Synergetic Innovation Center for Quantum Effects and Applications, Xiangjiang-Laboratory and Department of Physics, Hunan Normal University, Changsha 410081, China*

[2]*Institut für Theoretische Physik and IQST, Albert-Einstein-Allee 11, Universität Ulm, D-89081 Ulm, Germany*

(Received 7 September 2023; revised 5 March 2024; accepted 6 May 2024; published 20 May 2024)

In a theoretical study, we investigate the spin dynamics of interacting nitrogen-vacancy (NV) centers and quadrupolar $I = 3/2$ nuclear spins, specifically ^{11}B spins in hexagonal boron nitride (h-BN) nanosheets located near the microdiamond surface. We demonstrate the possibility of obtaining external spin-polarization by magnetic-field sweeps across the level anticrossings around zero field. To achieve this, we leverage crystal strains to establish a polarization transfer mechanism that remains robust against variations in NV orientation, crystal strain inhomogeneity, and electron-nuclear effective couplings. These results pave the way for hyperpolarization of spins in nanomaterials near the diamond surface without experiencing polarization loss to intrinsic nuclear spin-1/2 species, such as ^{13}C and ^{1}H nuclear spins in diamond. The ^{11}B spins in h-BN nanosheets, with their extended relaxation time and large surface area, present a promising alternative for relayed nuclear polarization to the liquid phase and for the development of quantum simulators based on surface nuclear spins.

DOI: 10.1103/PhysRevB.109.L180102

Introduction. Nuclear magnetic resonance (NMR) is a powerful versatile technique to address a wide range of fields in chemistry, biology, and medicine. Conventional NMR detection performed with inductive coils, requires high magnetic field and large detection volume to improve the signal-to-noise ratio (SNR) and spectral resolution. Nuclear polarization is determined by thermal (Boltzman) polarization, which is exceedingly low, around 10^{-5} for hydrogen spins and 3-T magnetic field at room temperature. Hence, several hyperpolarization methods have been proposed to enhance this polarization [1–4]. Nitrogen-vacancy (NV) centers in diamond [5–7] are examples of optical hyperpolarizing agents that can achieve almost perfect spin polarization through optical pumping, independent of the magnetic field, enabling hyperpolarization on nearby nuclei in bulk diamond [8–11], micro and nanodiamonds [12–14].

The investigation of optically "hyperpolarized nanodiamonds" is a long-standing and highly interesting research area because nanoscale or microscale particles of diamond in powdered form offer a significantly larger contact surface area [15]. Several control protocols have been proposed for ^{13}C spin hyperpolarization intrinsic to the micro and nanodiamond, such as PulsePol sequences [16], microwave (MW) [17–21] or magnetic field sweeps [22–24]. These approaches have been demonstrated in recent proof-of-principle experiments. However, achieving bulk polarization is only the first step. Subsequent stages involve the slow process of polarization diffusion toward the surface and then the transfer to external spins in the liquid phase. Unfortunately, these steps can be hindered by the presence of $P1$ centers and other paramagnetic impurities in diamond. In other words, the transfer of ^{13}C polarization to external spins is prevented by dark spins on the surface.

On the other hand, while some evidence for the efficient transfer of polarization from an NV center, which lacks strong couplings, to a dense layer of nuclear spins has already been provided with single crystalline diamond [25–27], no external spin hyperpolarization has been demonstrated yet, mainly due to low diamond surface-to-volume ratios. Although there have been theoretical advancements in polarization transfer to external nuclear spins in contact with powdered diamond [28], several significant challenges have been identified. These challenges include the following: large broadening of the electronic linewidth due to unavoidable misalignment between the applied magnetic field and the NV symmetry axis, relatively large distance between NV centers and target nuclei, short decoherence time of NV spins in small sizes of nanodiamonds [29] or the lack of nuclear spin species selectivity of polarization protocols. In this study, we propose a protocol to overcome these challenges and achieve robust polarization buildup in quadrupolar nuclei in nanomaterials near the microdiamond surface. Specifically, we focus on $I = 3/2$ ^{11}B boron spins in hexagonal boron nitride (h-BN) [30–32] nanosheets, utilizing a shallow NV center ensemble (2–5 nm depth to diamond surface) at zero-to-low-field.

Unlike traditional methods that ignore crystal strain, in this study we employ crystal strain near diamond surfaces as an asset that imparts robustness. The crystal strain is induced by local deformation of the diamond crystal, resulting in inhomogeneous broadening, typically in the range of 100 kHz in single-crystal diamond. However, in diamond powder and in shallow NV defects hosted in nanodiamonds, the

*These authors contributed equally.
†qchen@hunnu.edu.cn

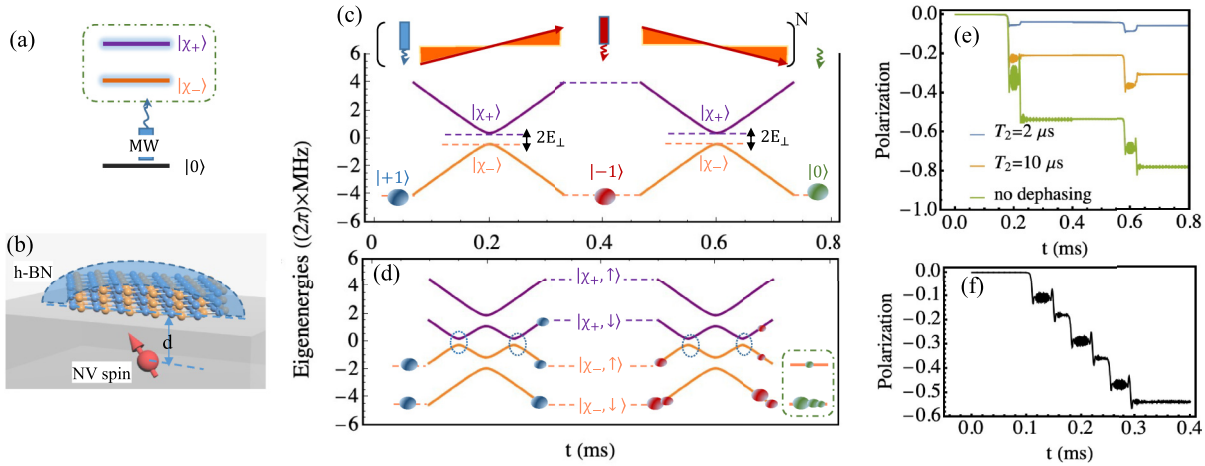

FIG. 1. Basic protocol of ^{11}B spin polarization mechanism around zero field. (a) The initial polarization subspace of the NV spin. (b) A shallow NV spin, at depth d below the diamond surface, is interacting with a h-BN nanosheet near the diamond surface. (c) Energy diagram of an isolated NV electron spin for a full magnetic-field cycle based on Eq. (1), which includes two magnetic-field sweeps, from negative to positive, and then back to negative field strength (orange). Squares in different colors indicate laser pulses and a microwave (MW) pulse to initial NV spin in state $|\chi_-\rangle$ ($|\chi_-\rangle \sim |m_s = +1\rangle$ (blue) or $|\chi_-\rangle \sim |m_s = -1\rangle$ (red). (d) Schematic energy diagram for the NV and a ^{11}B nuclear spin based on Eq. (2). Spin populations are represented by solid ellipses of variable radius; for clarity, we assume the NV spin is always fully initialized into $|\chi_-\rangle$, though only partial initialization is required. In both of the sweeps, there are two avoided crossings where population transfer takes place between $|\chi_-, \uparrow\rangle$ and $|\chi_+, \downarrow\rangle$. (e) Polarization of ^{11}B nuclear spins within a sweep cycle is shown by considering different coherence time T_2 of the NV spin and the duration of the LZ transition is $\tau \approx 2$ μs. The quadrupole splitting constant $\bar{Q} = (2\pi) \times 2.9$ MHz, the strength of crystal strain $E_\perp = (2\pi) \times 0.4$ MHz, the effective perpendicular coupling between NV and nuclear spins $a_x = (2\pi) \times 47$ kHz (the NV depth is assumed as 2 nm), the sweep rate $v = (2\pi) \times 30$ MHz/ms and $\omega(t = 0) = -(2\pi) \times 6$ MHz. (f) The effect of ^{14}N nuclear spins is included. The other parameters are the same during simulations for different color lines in (e).

inhomogeneous broadening can be even larger, reaching a few MHz [33–35]. Remarkably, our protocol avoids polarization loss to other nuclear spin-1/2 species and achieves robust polarization transfer to ^{11}B spins over a broad set of strain inhomogeneity, electron-nuclear couplings, and relative orientations of the NV axis and magnetic fields. The exceptional long relaxation time of ^{11}B spins, that can reach $T_{1b} = 175$ s [30] in h-BN nanosheets with thickness ∼50–100 nm and diameter 1 μm as well as the large surface area of the nanosheets benefit our polarization scheme. They may also provide a mediator to transfer the polarization to external molecules in solution. Additionally, our work provides a method for the initialization of quantum simulators based on surface nuclear spins [36–38].

The model. Our target samples are ^{11}B spins ($I = 3/2$) in hexagonal boron nitride (h-BN) nanosheets at the diamond surface interacting with shallow NV spins (∼2–5 nm), see Fig. 1(b). As a reasonable basic model we use an NV center interacting with a nearby ^{11}B nuclear spin with the effective coupling $a_x \in (2\pi) \times [0.01, 0.05]$ MHz [39,40]. For clarity, we initially assume that the magnetic field is aligned with the NV orientation, and the applied magnetic field is sufficiently small to induce degenerate states $|m_I = \pm 1/2\rangle$ and $|m_I = \pm 3/2\rangle$ of the ^{11}B nuclei.

We initialize the NV center in a highly polarized state in the $|m_s = \pm 1\rangle$ manifold, and gradually sweep the magnetic field across zero to the opposite direction which will transfer the NV polarization to the pseudo two-level system ^{11}B spins consisting of the of degenerate states $|\downarrow\rangle = |m_I = \pm 1/2\rangle$ and $|\uparrow\rangle = |m_I = \pm 3/2\rangle$. Close to zero magnetic field, we have

$$H_{NV} = \omega(t)\sigma_z + E_\perp \sigma_x, \tag{1}$$

where $\omega(t) = \omega_0 + vt$ is determined by the magnetic field with the initial frequency ω_0 and field sweep rate v, $E_\perp$ is the perpendicular component of the crystal strain, with $\sigma_z = |m_s = +1\rangle\langle m_s = +1| - |m_s = -1\rangle\langle m_s = -1|$ and $\sigma_x = |m_s = +1\rangle\langle m_s = -1| + |m_s = -1\rangle\langle m_s = +1|$. Eigenstates of the NV spin are given by $|\chi_\pm(t)\rangle = \pm\cos\frac{\eta}{2}|m_s = \pm 1\rangle + \sin\frac{\eta}{2}|m_s = \mp 1\rangle$ with $\sin\eta = E_\perp/\sqrt{\omega^2(t) + E_\perp^2}$.

Our scheme starts with a magnetic field initialized to an orientation opposite to that of the NV such that $\omega(t = 0) = -(2\pi) \times 6$ MHz. The NV spin is initialized into state $|m_s = 0\rangle$ by using laser illumination and then transferred to eigenstate $|\chi_-\rangle$ approximated as $|m_s = +1\rangle$ through a suitably tuned microwave (MW) pulse as shown in Fig. 1(c). The same MW pulse will also induce state transfer to $|\chi_-\rangle$ approximated as $|m_s = -1\rangle$ when the initial magnetic field direction is along the NV axis. The NV spin is reinitialized in state $|\chi_-\rangle$ after every sweep and a repetition of these processes gives negative polarization of ^{11}B spins in state $|\downarrow\rangle$ thanks to a dynamics that will be described in the following.

According to Landau-Zener (LZ) theory, when we initialize an isolated NV spin into state $|m_s = +1\rangle$ at the start of the sweep with $\omega(t = 0) = -(2\pi) \times 6$ MHz, a fully adiabatic slow passage, satisfying the adiabatic condition $4E_\perp^2/v \gg 1$, would transfer the NV spin to state $|m_s = -1\rangle$ at the end of the sweep [see Fig. 1(c)].

To understand the polarization mechanism, due to the coupling of the NV to the ^{11}B nuclei during quasiadiabatic sweep we consider the energy diagram of the NV-^{11}B system by using the NV-^{11}B coupling Hamiltonian as

$$H_1 = \omega_e \sigma_{\tilde{z}} + \frac{\bar{Q}}{2} I_{\tilde{z}} + H_{\text{int}}, \tag{2}$$

in which $\sigma_{\tilde{z}} = \frac{1}{2}(|\chi_+\rangle\langle\chi_+| - |\chi_-\rangle\langle\chi_-|)$ and $I_{\tilde{z}} = \frac{1}{2}(|\uparrow\rangle\langle\uparrow| - |\downarrow\rangle\langle\downarrow|)$, $\omega_e = 2\sqrt{\omega^2(t) + E_\perp^2}$, quadrupole coupling constant $\bar{Q} = (2\pi) \times 2.9$ MHz and $H_{\text{int}} = 2(\sigma_{\tilde{z}} \cos\eta - \sigma_{\tilde{x}} \sin\eta) \cdot (\sqrt{3} a_x I_{\tilde{x}} + 2 a_z I_{\tilde{z}})$ describes the dipole-dipole interaction between NV and ^{11}B spins. A full polarization transfer cycle includes the sequential application of negative-to-positive and positive-to-negative magnetic field sweeps, in which the NV spin is initialized into state $|\chi_-\rangle$ at each sweep start.

By initializing the NV spin into state $|\chi_-\rangle$, for each magnetic field sweep, the state $|\chi_-, \downarrow\rangle$ is not affected as its dynamics remains adiabatic ($4E_\perp^2/v \gg 1$), while the initial state $|\chi_-, \uparrow\rangle$ will have a probability for flipping to $|\chi_+, \downarrow\rangle$. This is the crucial key of the polarization transfers, when Hartmann-Hahn condition

$$\omega_e = 2\sqrt{\omega^2(t) + E_\perp^2} = \frac{\bar{Q}}{2} \tag{3}$$

could be matched at each of the avoided crossings. As shown in Fig. 1(d), if we have $0 < |E_\perp| < \frac{\bar{Q}}{4}$, there are sequential two avoided crossings of the energy levels for a negative-to-positive or positive-to-negative sweep, and the energy gap of the non-zero-field avoided crossing is given by $\sqrt{3} a_x \sin\eta$. The sweep rate is chosen to be partially nonadiabatic Landau-Zener (LZ) dynamic around the avoided crossing [blue dotted ellipses in Fig. 1(d)] with LZ transition probability $p_l \sim \exp(-2\pi\mu)$ with $\mu = 3a_x^2 \sin^2\eta/(8v\cos\eta)$ between the eigenstates $|\chi_-, \uparrow\rangle$ and $|\chi_+, \downarrow\rangle$. This probability is given by $P_l = P \sin^2[\Phi]$ with

$$P = 4p_l(1 - p_l), \tag{4}$$

and the phase Φ is related to parameters in both of adiabatic and nonadiabatic evolutions in the system [40–42]. Therefore, the net nuclear polarization buildup depends on the coherent population transfer around every avoided crossings due to partially nonadiabatic LZ transition probabilities. For an initial state of the NV given by $|\chi_-\rangle$ and assuming the ^{11}B nuclei unpolarized, the polarization cycle results in negative polarization of ^{11}B spins in state $|\downarrow\rangle$ regardless of the magnetic-field sweep direction, as confirmed by direct numerical simulations both for negative-to-positive and positive-to-negative field sweeps [as shown in Fig. 1(e)]. Initialization of the NV spin into state $|\chi_+\rangle$ induces positive nuclear polarization to state $|\uparrow\rangle$.

Robustness. Regarding each avoided crossing as a coherent process, as shown in Fig. 1(e), polarization is transferred under the condition $\tau < T_2(\text{NV})$, where $T_2(\text{NV})$ denotes the NV coherence lifetime, and $\tau \sim \sqrt{3} a_x |\sin\eta|/(2v|\cos\eta|)$ is the characteristic LZ time to coherent transfer. An accurate description of the system spin dynamics during a single magnetic-field sweep, in which the coupling of NV and ^{14}N nuclear spin is included, is presented in Fig. 1(f). We find that the interactions between NV and ^{14}N nuclear spins do not change the efficiency of nuclear polarization mechanism of ^{11}B nuclei (detailed calculations are included in the Supplemental Materials [40]).

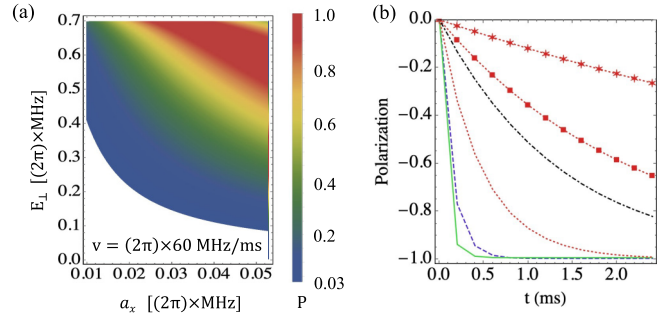

FIG. 2. The robustness of our scheme. (a) Transfer probability P as a function of the coupling strengths and crystal strains to show the robustness. (b) Polarization is transferred to a ^{11}B spin by assuming $E_\perp = (2\pi) \times 0.65$ MHz with $a_x = (2\pi) \times 0.012$(black dot-dashed); 0.035(blue dashed); 0.047(green) MHz. The red dotted lines present $a_x = (2\pi) \times 0.02$ MHz with $E_\perp = (2\pi) \times 0.65$(no marks); 0.45(cubes); 0.25(stars) MHz.

In practice, polarization transfer will involve a large ensembles of NV spins and target ^{11}B nuclei. We study this situation by considering the case of polarization of nuclear spins in h-BN nanosheets on a microdiamond surface with an ensemble of shallow NV centers. Because the Stoke phase Φ is sensitive to system parameters and is assumed to be averaged as $\langle\sin^2[\Phi]\rangle \approx 1/2$ [17,42], we calculate P as a function of both the strain components and the NV-^{11}B couplings to estimate the robustness of the parameter ranges, as shown in Fig. 2(a) and the Supplemental Material [40]. For simplicity, we first assume the magnetic field is along NV's orientation. Remarkably, according to our theory, it shows polarization transfer when $E_\perp$ is comparable to but not larger than $\frac{\bar{Q}}{4}$. Therefore, we have polarization transfer over a broad set of NV-^{11}B effective couplings and strain components, which is confirmed by our exact numerical simulations, as shown in Fig. 2(b).

Finally, we investigate the nuclear polarization efficiency as a function of the magnetic -field orientation relative to the NV centers in diamond powders, in which the Hamiltonian of an NV spin is

$$H_\theta = [\delta_b + \omega_\theta(t)]\sigma_z + E_\perp \sigma_x, \tag{5}$$

here $\omega_\theta(t) = \omega(t)\cos\theta$ with angle θ between NV's orientation and magnetic field, and δ_b is inhomogeneous broadening induced by interactions with electron and nuclear spins nearby the NV center. We assume $v = (2\pi) \times 60$ MHz/ms and average 300 runs to have the averaged polarization transfer of ^{11}B spins by considering different couplings to the NV spin, inhomogeneities of the longitudinal and transversal component of the crystal strain $E_z \in (2\pi) \times [-0.73, 0.73]$ MHz, $E_\perp \in (2\pi) \times [-1.5, 1.5]$ MHz and $\delta_b \in (2\pi) \times [-3, 3]$ MHz of approximate Gaussian probability distributions $p(g) = \frac{1}{\sqrt{2\pi}\sigma_g} \exp(-g^2/2\sigma_g^2)$ with $\sigma_g/(2\pi) = 0.25$, 0.5 or 1 MHz corresponding to $g = E_z$, $E_\perp$ or δ_b. As shown in Fig. 3(c), the spin dynamics is insensitive to the exact start and end magnetic-field values, numerical simulations of the averaged

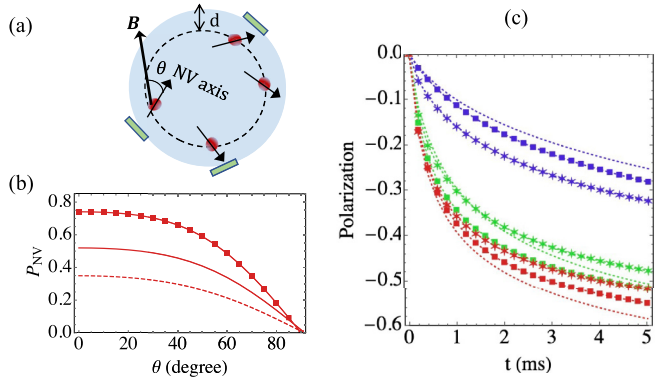

FIG. 3. The polarization buildup of ^{11}B spins in h-BN nanosheets by considering a solid mixture of microdiamonds (diameter $>1\mu$m) and h-BN nanosheets (diameter $<1\mu$m). (a) NV centers are $d \sim 2$–5 nm depth from the microdiamond surface and h-BN nanosheets are covered on the surface. (b) The ensemble-averaged initial polarization of the NV centers regarding the angle θ between their orientations and magnetic field by assuming 300 times averaging in random values within $E_z \in (2\pi) \times [-0.73, 0.73]$ MHz and and $\delta_b = (2\pi) \times 0$(red cubes), $\in (2\pi) \times [-2, 2]$(red solid), [-3, 3](red dashed) MHz, MW Rabi frequency is given by $(2\pi) \times 8$ MHz and the ensemble-averaged initial polarization is an average over all the possible angles between NV axis and MW field [40]. (c) Polarization transfer simulation by assuming 300 times averaging in random values within $E_\perp \in (2\pi) \times [-1.5, 1.5]$ MHz and $\delta_b \in (2\pi) \times [-3, 3]$ MHz. Three different angles are given $\theta = 0^\circ$ (dashed line), 40° (cubes), and 75° (stars) corresponding to couplings $a_x = (2\pi) \times 0.012$(blue); 0.026(green); 0.047(red) MHz.

polarization transfers show similar performances regardless of NV orientation variance and δ_b values [40]. The MW initialization of polarization NV centers, defined as population difference between states $|+1\rangle$ and $|-1\rangle$ [40] is also a limiting factor of the final polarization, as shown in Fig. 3(b), although inhomogeneous broadening δ_b and longitudinal component of the crystal strain E_z has almost no effect in the polarization transfer in our method, they are related to polarization initialization of the NV centers. We have $P_{\rm NV} > 0.1$ when $\theta = 80^\circ$, and therefore conclude our method is confined to the solid cone defined by $\theta > 80^\circ$, which includes 83% of NV orientations.

By assuming a solid mixture of microdiamonds and h-BN nanosheets with the same volume concentrations as 1:1, we can estimate the final polarization $\bar{P}_b \approx \rho_{\rm NV} T_o P_1 / \rho_n$ with $T_o =$ 100 s the total cycle time, NV density $\rho_{\rm NV} = 1.6 \times 10^4$ μm^{-3} and ^{11}B spin density $\rho_n = 1.6 \times 10^{10}$ μm^{-3}. When $d \sim 2$ nm, our mechanism gives polarization rate as $P_1 \sim 0.17/(0.2\,\text{ms})$ [see Fig. 3(b)], and we have the final polarization $\bar{P}_b \approx 8.5\%$. A similar estimation of the $d \sim 5$ nm case gives 2% of ^{11}B spins to be polarized. Although we study of ^{11}B spins in h-BN nanosheets, our method could be used for polarization of the other quadrupolar nuclei and materials, i.e., ^{27}Al spins in Al_2O_3 nanoparticles. Before concluding, we would like to mention that our polarization mechanism shares some similarities with other methods of MW sweeps and field sweeps. However, in our scheme, NV spin works as a pseudo two-level system constituted of states $|m_s = \pm 1\rangle$ so that there is no similar hierarchical gaps of NV and ^{13}C spins encountered in Ref. [18]. Moreover, we take advantage of the transverse zero-field splitting induced by the strain to impart robustness. The principles of our protocol allow for extension to other systems where transverse zero-field splitting exists and thus open a much wider field of application. Specifically, molecular color centers, which have gained growing interest in recent years [43,44], owns a noticeable transverse zero-field splitting due to low symmetry. We provide a general method to polarize quadrupolar nuclei in nanomaterials out of the diamond without the polarization loss to ^{13}C spins in diamond, which opens another way for chemical and structural analysis of nanomaterials or other compounds surface layers on microdiamonds through enhancing NMR spectroscopy around zero field. Low magnetic field gives a relative small sweep range that leads to fast polarization transfers, and 83% of NV orientations giving contributions to polarization transfer. Although low magnetic field leads to a smaller relaxation time of nuclei, comparing with previous sweep schemes to polarize ^{13}C spins in microdiamonds, paramagnetic $P1$ centers in diamond reduce relaxation time T_{1c} of ^{13}C spins in diamond dramatically [45], but have small effects to ^{11}B spins due to their large quadrupolar couplings.

Conclusion. In summary, we present a nuclear polarization mechanism applicable to diamond powder mixtures, enabling direct polarization of quadrupolar nuclear spin targets outside the diamond crystal instead of ^{13}C spins within diamond. Central to this approach is utilization of Landau-Zener dynamics induced by quasiadiabatic magnetic field sweeps across the set of avoided crossings, which arise from nearly matched energy differences of the individual NV and ^{11}B spins. This technique can operate under ambient conditions, and remains robust to strain inhomogeneity, spin coupling heterogeneity and NV orientation disorder. Hyperpolarization of ^{11}B spins in nanosheets offers a combination of long relaxation time and large surface area, making it an excellent alternative for a mediated nuclear polarization medium. Our work introduces another promising platform for exploiting NV based hyperpolarization to achieve optically hyperpolarized nanomaterials in solid phase and in a liquid at room temperature.

Acknowledgments. We thank Fedor Jelezko for comments on the manuscript. Q.C. is supported by the National Natural Science Foundation of China (Grants No. 12375012, and No. 12247105), Hunan Provincial Major Science and Technology Program (Grant No. 2023ZJ1010), and Hunan provincial major sci-tech program (XJ2302001). M.B.P. was supported by the European Research Council Synergy Grant HyperQ (Grant No. 856432) and the BMBF Zukunftscluster QSense: Quantensenoren für die biomedizinische Diagnostik (QMED) (Grant No. 03ZU1110FF).

[1] C. R. Bowers and D. P. Weitekamp, Phys. Rev. Lett. **57**, 2645 (1986).

[2] C. R. Bowers and D. P. Weitekamp, J. Am. Chem. Soc. **109**, 5541 (1987).

[3] J. H. Ardenkjær-Larsen, B. Fridlund, A. Gram, G. Hansson, M. H. Lerche, R. Servin, M. Thaning, and K. Golman, Proc. Natl. Acad. Sci. USA **100**, 10158 (2003).

[4] T. R. Eichhorn, A. J. Parker, F. Josten, C. Müller, J. Scheuer, J. M. Steiner, M. Gierse, J. Handwerker, M. Keim, S. Lucas, M. U. Qureshi, A. Marshall, A. Salhov, Y. Quan, J. Binder, K. D. Jahnke, P. Neumann, S. Knecht, J. W. Blanchard, M. B. Plenio *et al.*, J. Am. Chem. Soc. **144**, 2511 (2022).

[5] M. W. Doherty, N. B. Manson, P. Delaney, F. Jelezko, J. Wrachtrup, and L. C. Hollenberg, Phys. Rep. **528**, 1 (2013).

[6] F. Jelezko and J. Wrachtrup, Physica Status Solidi (a) **203**, 3207 (2006).

[7] Y. Wu, F. Jelezko, M. B. Plenio, and T. Weil, Angew. Chem. Int. Ed. **55**, 6586 (2016).

[8] P. London, J. Scheuer, J.-M. Cai, I. Schwarz, A. Retzker, M. B. Plenio, M. Katagiri, T. Teraji, S. Koizumi, J. Isoya, R. Fischer, L. P. McGuinness, B. Naydenov, and F. Jelezko, Phys. Rev. Lett. **111**, 067601 (2013).

[9] R. Fischer, C. O. Bretschneider, P. London, D. Budker, D. Gershoni, and L. Frydman, Phys. Rev. Lett. **111**, 057601 (2013).

[10] V. Jacques, P. Neumann, J. Beck, M. Markham, D. Twitchen, J. Meijer, F. Kaiser, G. Balasubramanian, F. Jelezko, and J. Wrachtrup, Phys. Rev. Lett. **102**, 057403 (2009).

[11] G. A. Álvarez, C. O. Bretschneider, R. Fischer, P. London, H. Kanda, S. Onoda, J. Isoya, D. Gershoni, and L. Frydman, Nat. Commun. **6**, 8456 (2015).

[12] K. Miyanishi, T. F. Segawa, K. Takeda, I. Ohki, S. Onoda, T. Ohshima, H. Abe, H. Takashima, S. Takeuchi, A. I. Shames *et al.*, Magn. Reson. **2**, 33 (2021).

[13] A. Ajoy, R. Nazaryan, E. Druga, K. Liu, A. Aguilar, B. Han, M. Gierth, J. T. Oon, B. Safvati, R. Tsang *et al.*, Rev. Sci. Instrum. **91**, 023106 (2020).

[14] E. Rej, T. Gaebel, D. E. Waddington, and D. J. Reilly, J. Am. Chem. Soc. **139**, 193 (2017).

[15] T. Boele, D. Waddington, T. Gaebel, E. Rej, A. Hasija, L. Brown, D. McCamey, and D. Reilly, Phys. Rev. B **101**, 155416 (2020).

[16] I. Schwartz, J. Scheuer, B. Tratzmiller, S. Müller, Q. Chen, I. Dhand, Z.-Y. Wang, C. Müller, B. Naydenov, F. Jelezko, and M. B. Plenio, Sci. Adv. **4**, eaat8978 (2018).

[17] Q. Chen, I. Schwarz, F. Jelezko, A. Retzker, and M. B. Plenio, Phys. Rev. B **92**, 184420 (2015).

[18] A. Ajoy, K. Liu, R. Nazaryan, X. Lv, P. R. Zangara, B. Safvati, G. Wang, D. Arnold, G. Li, A. Lin *et al.*, Sci. Adv. **4**, eaar5492 (2018).

[19] A. Ajoy, R. Nazaryan, K. Liu, X. Lv, B. Safvati, G. Wang, E. Druga, J. Reimer, D. Suter, C. Ramanathan *et al.*, Proc. Natl. Acad. Sci. USA **115**, 10576 (2018).

[20] P. R. Zangara, S. Dhomkar, A. Ajoy, K. Liu, R. Nazaryan, D. Pagliero, D. Suter, J. A. Reimer, A. Pines, and C. A. Meriles, Proc. Natl. Acad. Sci. USA **116**, 2512 (2019).

[21] A. Ajoy, A. Sarkar, E. Druga, P. Zangara, D. Pagliero, C. A. Meriles, and J. A. Reimer, J. Magn. Reson. **331**, 107021 (2021).

[22] J. Henshaw, D. Pagliero, P. R. Zangara, M. B. Franzoni, A. Ajoy, R. H. Acosta, J. A. Reimer, A. Pines, and C. A. Meriles, Proc. Natl. Acad. Sci. USA **116**, 18334 (2019).

[23] P. R. Zangara, J. Henshaw, D. Pagliero, A. Ajoy, J. A. Reimer, A. Pines, and C. A. Meriles, Nano Lett. **19**, 2389 (2019).

[24] R. Wunderlich, R. Staacke, W. Knolle, B. Abel, J. Haase, and J. Meijer, J. Appl. Phys. **130**, 104301 (2021).

[25] D. A. Broadway, J.-P. Tetienne, A. Stacey, J. D. Wood, D. A. Simpson, L. T. Hall, and L. C. Hollenberg, Nat. Commun. **9**, 1246 (2018).

[26] A. Healey, L. Hall, G. White, T. Teraji, M.-A. Sani, F. Separovic, J.-P. Tetienne, and L. Hollenberg, Phys. Rev. Appl. **15**, 054052 (2021).

[27] P. Fernández-Acebal, O. Rosolio, J. Scheuer, C. Muller, S. Muller, S. Schmitt, L. P. McGuinness, I. Schwarz, Q. Chen, A. Retzker *et al.*, Nano Lett. **18**, 1882 (2018).

[28] Q. Chen, I. Schwarz, F. Jelezko, A. Retzker, and M. B. Plenio, Phys. Rev. B **93**, 060408 (2016).

[29] J. Tisler, G. Balasubramanian, B. Naydenov, R. Kolesov, B. Grotz, R. Reuter, J.-P. Boudou, P. A. Curmi, M. Sennour, A. Thorel *et al.*, ACS Nano **3**, 1959 (2009).

[30] A. M. Love, B. Thomas, S. E. Specht, M. P. Hanrahan, J. M. Venegas, S. P. Burt, J. T. Grant, M. C. Cendejas, W. P. McDermott, A. J. Rossini *et al.*, J. Am. Chem. Soc. **141**, 182 (2019).

[31] I. Lovchinsky, J. Sanchez-Yamagishi, E. Urbach, S. Choi, S. Fang, T. Andersen, K. Watanabe, T. Taniguchi, A. Bylinskii, E. Kaxiras *et al.*, Science **355**, 503 (2017).

[32] J. Henshaw, P. Kehayias, M. Saleh Ziabari, M. Titze, E. Morissette, K. Watanabe, T. Taniguchi, J. Li, V. M. Acosta, E. S. Bielejec *et al.*, Appl. Phys. Lett. **120**, 174002 (2022).

[33] M. E. Trusheim and D. Englund, New J. Phys. **18**, 123023 (2016).

[34] M. C. Marshall, R. Ebadi, C. Hart, M. J. Turner, M. J. Ku, D. F. Phillips, and R. L. Walsworth, Phys. Rev. Appl. **17**, 024041 (2022).

[35] S. Sharma, C. Hovde, D. H. Beck, and F. Alghannam, arXiv:1802.08767.

[36] F. T. Tabesh, M. Fani, J. S. Pedernales, M. B. Plenio, and M. Abdi, Phys. Rev. B **107**, 214307 (2023).

[37] J. Cai, A. Retzker, F. Jelezko, and M. B. Plenio, Nat. Phys. **9**, 168 (2013).

[38] X. Gao, S. Vaidya, K. Li, P. Ju, B. Jiang, Z. Xu, A. E. L. Allcca, K. Shen, T. Taniguchi, K. Watanabe *et al.*, Nat. Mater. **21**, 1024 (2022).

[39] J.-P. Tetienne, L. Hall, A. Healey, G. White, M.-A. Sani, F. Separovic, and L. Hollenberg, Phys. Rev. B **103**, 014434 (2021).

[40] See Supplemental Material at http://link.aps.org/supplemental/10.1103/PhysRevB.109.L180102 for detailed calculations and simulations.

[41] S. Ashhab, J. Johansson, A. Zagoskin, and F. Nori, Phys. Rev. A **75**, 063414 (2007).

[42] S. N. Shevchenko, S. Ashhab, and F. Nori, Phys. Rep. **492**, 1 (2010).

[43] S. L. Bayliss, D. W. Laorenza, P. J. Mintun, B. D. Kovos, D. E. Freedman, and D. D. Awschalom, Science **370**, 1309 (2020).

[44] M. R. Wasielewski III, M. D. E. Forbes, N. L. Frank, K. Kowalski, G. D. Scholes *et al.*, Nat. Rev. Chem. **4**, 490 (2020).

[45] A. Ajoy, B. Safvati, R. Nazaryan, J. T. Oon, B. Han, P. Raghavan, R. Nirodi, A. Aguilar, K. Liu, X. Cai, X. Lv, E. Druga, C. Ramanathan, J. A. Reimer, C. A. Meriles, D. Suter, and A. Pines, Nat. Commun. **10**, 5160 (2019).